

MonoSIM: An open source SIL framework for Ackermann Vehicular Systems with Monocular Vision

Shantanu Rahman*
Department of Electrical and
Electronic Engineering
Islamic University of Technology
Gazipur, Bangladesh
shantanurahman@iut-dhaka.edu

*Corresponding author

Nayeb Hasin
Department of Electrical and
Electronic Engineering
Islamic University of Technology
Gazipur, Bangladesh
nayebhasin@iut-dhaka.edu

Mainul Islam
Department of Electrical and
Electronic Engineering
Islamic University of Technology
Gazipur, Bangladesh
mainulislam@iut-dhaka.edu

Md. Zubair Alom Rony
Department of Electrical and
Electronic Engineering
Islamic University of Technology
Gazipur, Bangladesh
zubairalom@iut-dhaka.edu

Golam Sarowar
Department of Electrical and
Electronic Engineering
Islamic University of Technology
Gazipur, Bangladesh
asim@iut-dhaka.edu

Abstract—This paper presents an open-source Software-in-the-Loop (SIL) simulation platform designed for autonomous Ackermann vehicle research and education. The proposed framework focuses on simplicity, while making it easy to work with small-scale experimental setups, such as the XTENTH-CAR platform. The system was designed using open source tools, creating an environment with a monocular camera vision system to capture stimuli from it with minimal computational overhead through a sliding window based lane detection method. The platform supports a flexible algorithm testing and validation environment, allowing researchers to implement and compare various control strategies within an easy-to-use virtual environment. To validate the working of the platform, Model Predictive Control (MPC) and Proportional–Integral–Derivative (PID) algorithms were implemented within the SIL framework. The results confirm that the platform provides a reliable environment for algorithm verification, making it an ideal tool for future multi-agent system research, educational purposes, and low-cost AGV development. Our code is available at <https://github.com/shantanu404/monosim.git>.

Index Terms—Software-in-the-Loop (SIL), Monocular Vision, Lane Detection, Ackermann Steering, Model Predictive Control (MPC), PID Control, Robot Operating System (ROS2), Vision-Based Navigation, Autonomous Ground Vehicles (AGV)

I. INTRODUCTION

Autonomous vehicles are quickly becoming a key transportation technology. Companies like Tesla are accelerating development and increasing market demand. In many developed countries, users are beginning to depend on these systems [1]. Since human error remains a major cause of road accidents, autonomous driving offers a promising pathway toward improved safety [2]. Motivated by these trends, we

introduce MonoSIM, a lightweight and accessible simulation testbed designed to support research on autonomous vehicle navigation.

MonoSIM is built on top of the Robot Operating System (ROS) and the MVSIM simulator [3], which incorporates the Box2D physics engine. Through this design, MonoSIM enables lane-tracking experiments using monocular vision and widely used control algorithms. The framework provides telemetry extraction, real-time sensor emulation, and a flexible environment for developing low-level vision pipelines—capabilities that are often restricted in traditional control-focused simulators. MonoSIM places emphasis on real-time sensor data processing, dynamic region-of-interest extraction for lane detection, sliding-window techniques, quadratic curve fitting, and improved transparency of the simulation environment. Practical constraints such as limited computational power and low-resolution camera input are also taken into consideration within the system’s design.

Several prior works have proposed testbeds for autonomous systems. Jiang et al. integrated an MPC framework with a learning-based error estimator using offline data [4]. Bhadani et al. developed the “CAT Vehicle Testbed” using ROS and Gazebo to support hardware-in-the-loop experimentation [5]. Sarantinoudis et al. presented a ROS-based platform supporting V2V and V2I communication [6]. Elmoghazy et al. proposed an edge-enhanced V2X testbed using an F1Tenth-scale vehicle [7]. Bouchemal et al. constructed a real-world DSRC-based V2X infrastructure [8]. Additional contributions include fault-simulation platforms [9], large-scale heterogeneous testbeds [10], controlled-environment autonomous pro-

arXiv:2603.23965v1 [cs.RO] 25 Mar 2026

totypes [11], reconfigurable multi-sensor platforms [12], radar-focused MATLAB testbeds [13], integrated UAV-UGV environments [14], and digital-twin-supported hybrid testbeds [15].

Compared to these existing platforms, MonoSIM offers lower computational demands and improved scalability for testing and comparing autonomous vehicle control algorithms within a unified monocular-vision-driven simulation environment.

II. METHODOLOGY

Sensors and locomotion are necessary to make interaction with the environment. In our testbed, we used a monocular camera (*Logitech c310 HD*) to observe the environment around. For actuation, the car model we developed, follows the mathematical model of ackermann steering using an approximation of the bicycle model. Ackermann steering helps to turn a car by adjusting the rotating angle of wheels according to their position where, The bicycle model simplifies the vehicle’s dynamics by representing the vehicle with a single front wheel and a single rear wheel.

A. CALIBRATION

For consistent processing, a frame from the target environment was taken and enlarged to 640×480 pixels. OpenCV was used to convert the image from BGR to RGB format for viewing.

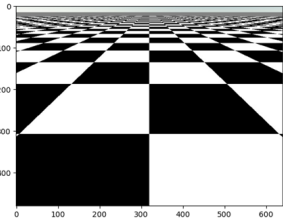


Fig. 1: Original input frame

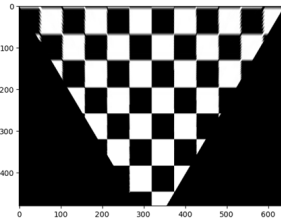


Fig. 2: Birds Eye View

A homography-based perspective transformation was used to create a top-down view. After the source and destination points were manually specified, the Direct Linear Transformation algorithm was used to calculate the transformation matrix. After that, the picture was distorted to a corrected viewpoint.

The calibration was performed using a 5×4 chessboard. Using OpenCV’s `findChessboardCorners` with adaptive thresholding and normalizing for enhanced robustness, chessboard corners were identified after the corrected image was converted to grayscale.

Corner positions were refined to subpixel accuracy using `cornerSubPix`, and the results were visualized for verification. The corner coordinates were reshaped to evaluate geometric consistency, and average spacing between adjacent corners was computed in both horizontal and vertical directions.

Finally, the homography matrix was printed and confirmed. This matrix provides a geometric mapping between original and rectified views and is essential for applications such as camera calibration, navigation, and ground plane analysis.

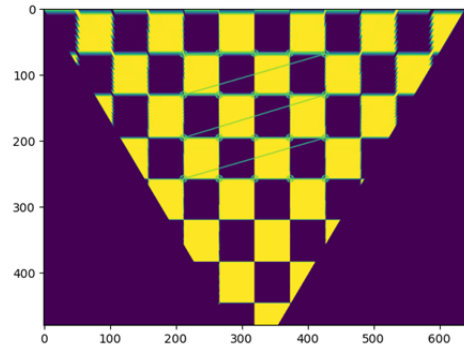


Fig. 3: Detected and refined chessboard corners overlaid on the grayscale image.

B. LANE DETECTION

The feature-based lane detection pipeline uses edges and local visual cues such as gradients and intensity variations, which remain stable across different road geometries but may vary with illumination. The camera output is first resized to 640×480 and undistorted using the intrinsic camera matrix obtained by camera calibration.

Because fitting polynomials directly on the perspective image would require high-order models, a bird’s-eye view transform is applied [16] to make the lanes parallel and fit them using a second or third-order polynomial (see Fig. 4 and Fig. 5).

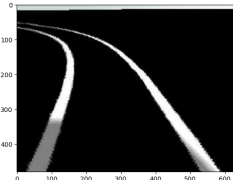


Fig. 4: Lane visible in camera

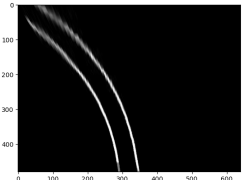


Fig. 5: Bird's Eye view

After warping, the image is converted to HSV, and lane features are isolated primarily from the Value channel. The lower half of this channel is processed using Gaussian blurring, thresholding, and morphological filters. A vertical histogram of pixel intensities is then used to estimate the initial left and right lane positions

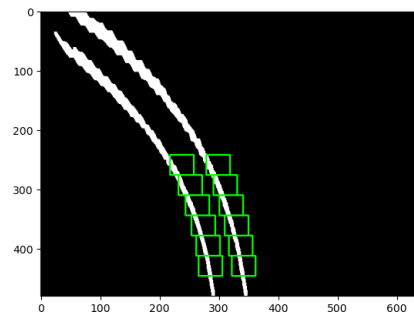


Fig. 6: Implementation of Sliding window technique

Lane pixels are extracted using a sliding-window method, where windows move upward along the image to collect connected lane points. Separate polynomials are fitted to the left and right lane boundaries, providing a continuous representation of lane geometry. (Fig. 6). An overview of the entire pipeline is shown in Fig. 7.

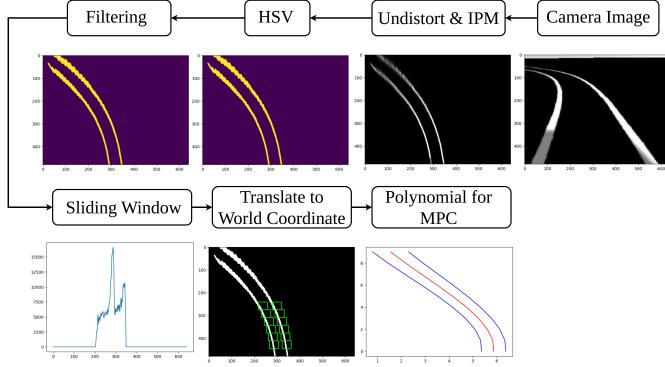


Fig. 7: Overall lane detection pipeline

C. VEHICLE DYNAMICS

Before developing our vehicle dynamics model, we are assuming only 3 DOF of motion for our autonomous vehicle i.e. lateral, longitudinal and yaw motion. We are also making some assumption based on 3 DOF motions which are as follows [17]:

- For the front and rear axles, the wheels are considered lumped together.
- Assuming fixed velocity for our autonomous vehicle
- Maneuvering only the front axel.
- The weight distribution is considered uniform throughout the body and extra dynamics such as suspension, aerodynamics, and slip factors are discarded

Considering Newton's Second Law of motion for 3 DOF [18], vehicle dynamics model can be constructed as :

$$m(\ddot{y} + \dot{x}\dot{\phi}) = 2(F_{yf} \sin \delta_f + F_{cf} \cos \delta_f) + 2F_{cr} \quad (1)$$

$$I_z \ddot{\phi} = 2b(F_{yf} \sin \delta_f + F_{cf} \cos \delta_f) - 2aF_{cr} \quad (2)$$

In the above equation Vehicle mass is denoted using m , inertia along z axis is denoted using I_z , ϕ and δ_f are the yaw and steering angle respectively. Distance from the center of gravity to the front and rear axels are denoted using b and a respectively.

Pacejka tire model [19] is applied in this paper, Where the cornering angle and slip ratio of tire are quite small, the linearized and simplified formulas of longitudinal force and lateral force in the tire model are given by:

$$F_{cf} = C_{cf} \alpha_f \quad (3)$$

$$F_{cr} = C_{cr} \alpha_r \quad (4)$$

where C_{cf} and C_{cr} are the front and the rear cornering tire stiffness coefficient, respectively. Similarly, α_f and α_r are the front and rear tire slip angles, respectively.

Real time performance can be improved and optimized by converting the nonlinear dynamic model into the state space model and linearized, where $\chi = \dot{x}, \dot{y}, \phi, \dot{\phi}^T$ is the state space vector and the control variable is $u = \delta_f$ [20] to increase the versatility of the model and approximate linearized model is formed.

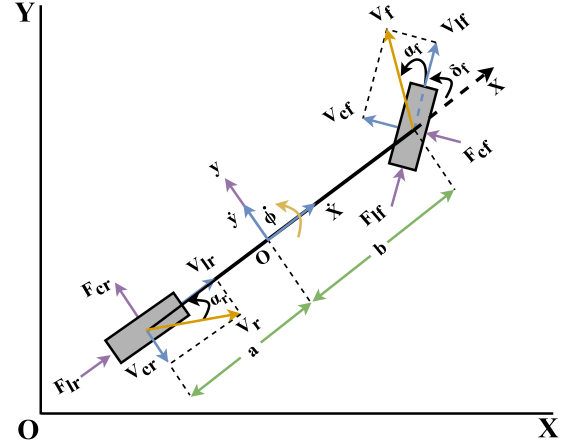


Fig. 8: Dynamics of Ackermann model

where

$$A_t = \left. \frac{\partial f(\chi, u)}{\partial \chi} \right|_{\chi=\chi_0; u=u_0} \quad (5)$$

$$B_t = \left. \frac{\partial f(\chi, u)}{\partial u} \right|_{\chi=\chi_0; u=u_0} \quad (6)$$

$$Y_t = \begin{bmatrix} \phi \\ Y \end{bmatrix} C_t = [1, 0, 0, 0]^T \quad (7)$$

Due to the continuous nature of the above equation, these equations cannot be applied directly into the model predictive control algorithm, so discretization is performed.

$$\chi(k+1) = A_k \chi(k) + B_k u(k) \quad (8)$$

$$Y(k) = C_k \chi(k) \quad (9)$$

D. STATE AND OUTPUT PREDICTION

In the process of path tracking, we need to predict the future behavior of vehicle in the specified prediction horizon, and calculate the control input in the next moment by minimizing the error between predictive variables and the references under various constraints. Given that the input of the model is the control increment $\Delta u(k)$ of the control signal $u(k)$, an incremental state space model is formulated as follows:

$$\tilde{\chi}(k+1) = \tilde{A}_k \tilde{\chi}(k) + \tilde{B}_k \Delta u(k) \quad (10)$$

$$\tilde{Y}(k) = \tilde{C}_k \tilde{\chi}(k) \quad (11)$$

Where the symbols retain their traditional meaning.

To forecast the system's state at future intervals, assuming the current sampling time is k , where $k > 0$, and the state variable vector $\tilde{\chi}(k)$ denotes the present system information.

The forthcoming control sequence is represented by $\Delta u(k + j) = 0$, where $j = N_c, N_c + 1, \dots, N_p - 1$. N_c and N_p denote the control and prediction horizons, respectively.

$$\Delta U_a(k) \triangleq \begin{bmatrix} \Delta u(k) \\ \Delta u(k+1) \\ \vdots \\ \Delta u(k+N_c-1) \end{bmatrix}_{(N_c \times 1)} \quad (12)$$

$$\tilde{\chi}(k+1|k) = \tilde{A}_k \tilde{\chi}(k) + \tilde{B}_k \Delta u(k)$$

$$\tilde{\chi}(k+2|k) = \tilde{A}_{k+1} \tilde{A}_k \tilde{\chi}(k) + \tilde{A}_k \tilde{B}_k \Delta u(k) + \tilde{B}_{k+1} \Delta u(k+1)$$

⋮

$$\begin{aligned} \tilde{\chi}(k+N_c|k) &= \alpha(k, N_c-1, 0) \tilde{\chi}(k) \\ &+ \alpha(k, N_c-1, 1) \tilde{B}_k \Delta u(k) \\ &+ \dots + \tilde{B}_{k+N_c-1} \Delta u(k+N_c-1) \end{aligned}$$

⋮

$$\begin{aligned} \tilde{\chi}(k+N_p|k) &= \alpha(k, N_p-1, 0) \tilde{\chi}(k) \\ &+ \alpha(k, N_p-1, 1) \tilde{B}_k \Delta u(k) \\ &+ \dots \\ &+ \alpha(k, N_p-1, N_c) \tilde{B}_{k+N_c-1} \Delta u(k+N_c-1) \end{aligned} \quad (13)$$

The prediction horizon is equal to or, often times, greater than the control horizon. Consequently, the prediction input vector $\Delta u_a(k)$ can be delineated.

State vector and output of every sample instance in the prediction horizon can be formulated in Eq 13. Using similar technique we can then calculate trajectory for any given set of input controls for the horizons.

E. CONSTRUCTION OF COST FUNCTION

The fundamental goal of the controller is to determine the sequence of control actions that will minimize the sum of the squared deviations of the expected output from the reference trajectory. This is the basic objective of the controller, the cost function can be defined as:

$$J_k = \left[\tilde{Y}_{(a,\text{ref})}(k) - \tilde{Y}_a(k) \right]^T Q \left[\tilde{Y}_{(a,\text{ref})}(k) - \tilde{Y}_a(k) \right] + \Delta U_a^T(k) R \Delta U_a(k) \quad (14)$$

The matrices that contain the weights of the inputs and outputs are denoted as Q and R . The matrix $\tilde{Y}_{(a,\text{ref})}(k)$ is the reference matrix. For this experiment they have been tuned manually.

III. EXPERIMENTAL SETUP

The validation of the proposed method is performed on an Ubuntu 24.04 LTS, equipped with a 12 generation Intel Core i7 mobile processor. To make sure we test the algorithms on isolation, we aimed to make the environment as abstract as possible to avoid any bias.

For that reason, we chose MVSIM as our simulation platform which boasts on its 2.5D capable simulation using Box2D engine [3]. ROS2 messaging service was used to communicate between the simulation and the algorithm process. ROS2 was chosen because it provided modularity and scalability to the system. The simulation was run in the above-mentioned setup together with some other ros2 nodes that collected odometry data for comparison with other algorithms. The graph in Fig. 9 shows all the components that were run in a standard experiment.

The environment was almost black and white with clearly defined lane lines to indicate the vehicle path. This was in turn detected from the environment using the described method in Section II-B. This process is analogous to the SOTA ML models segmenting the image into different lane lines. Together with some calibration data from the monocular camera, we were able to deduce the physical points in the actual world. This is again analogous to the case for ML models deducing the depth of pixels in the image. This allowed us to focus only on fine-tuning the underlying algorithm without being concerned with other external factors.

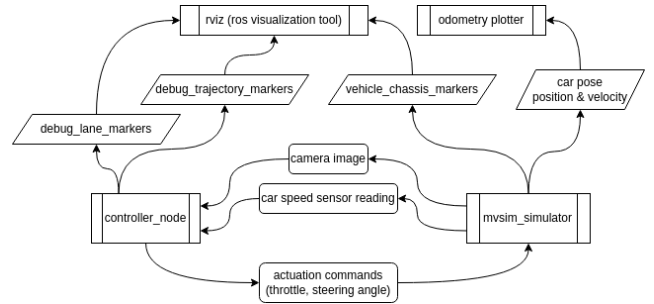


Fig. 9: Software Architecture of Simulation

The controller node is responsible for driving the car. It does so by sending the simulator program its desired throttle (acceleration) and steering angle in the form of a ros2 twist message. The controller derives these values from the input camera image and the car's speed using a simulated speedometer sensor located on the vehicle. The controller node then processes this information with the desired algorithm to dictate the throttle/brake and steering angle of the vehicle.

Figure 11 shows ROS2 rviz showing the monocular camera output along with the detected lane and the predicted path to follow. In Figure 10, we can see that MVSIM simulated world in isometric view.

Figure 12 shows a sample runtime information of the vehicle while running the simulation. The plots consecutively show its current position in world coordinates, the velocity and the heading angle along with its angular velocity.

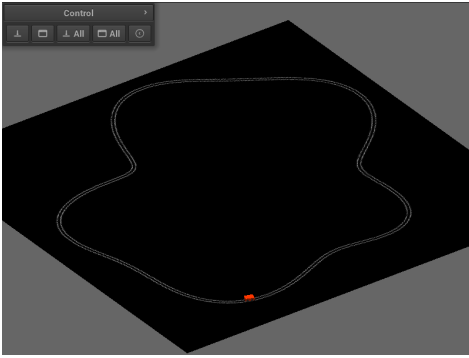


Fig. 10: MVSIM Simulation platform

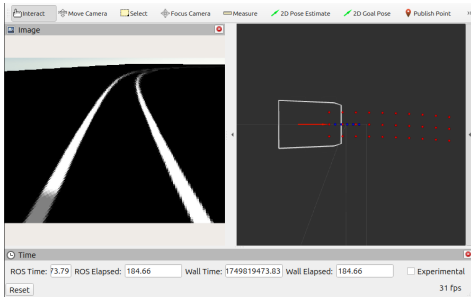


Fig. 11: RViz showing debugging information

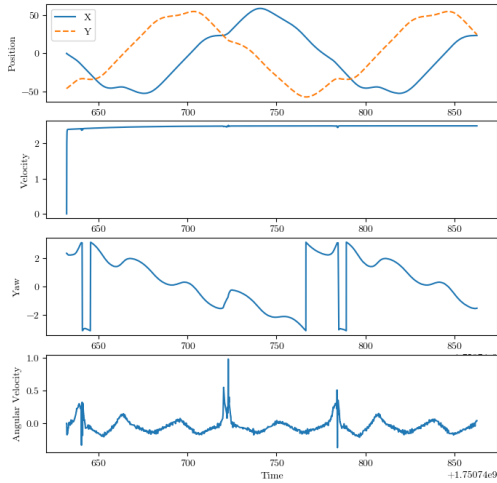


Fig. 12: Sample Runtime Information

IV. RESULTS & OBSERVATION

The experiment was conducted across multiple trials using randomly generated tracks of similar complexity, created by adding sinusoidal curvatures to a uniform circular path, as illustrated in Fig. 13. The initial velocity profiles of the vehicle for PID and MPC controllers are depicted in Fig. 14. Overall, both controllers demonstrated comparable performance; however, they each exhibit distinct operational characteristics. The PID controller maintained an almost constant velocity throughout each run, including sharp turns. The behavior produced apparent spikes in angular velocity, as shown in Fig.

15. In contrast, MPC produced smoother and more regulated control actions. Its adherence to state and input constraints, however, introduced oscillations in angular velocity (Fig. 16) and tracking error. Consequently, PID achieves lower trajectory deviation, while MPC provides more robust, constraint-aware control at the expense of some accuracy, as summarized in Table I.

TABLE I: Mean Squared Deviation from all of the runs

Metric	PID	MPC
Lateral Mean Squared Deviation	0.0136 m^2	0.0390 m^2
Angular Mean Squared Deviation	0.000548 rad^2	0.001014 rad^2

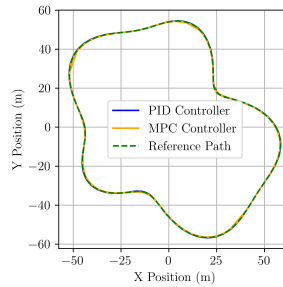


Fig. 13: Vehicle Trajectories in every run

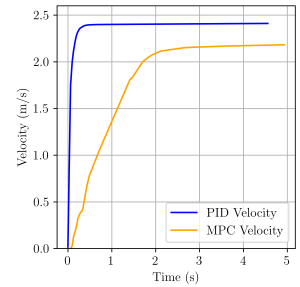


Fig. 14: Initial vehicle velocities

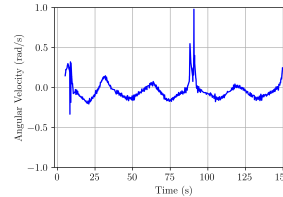


Fig. 15: Angular Velocity - PID

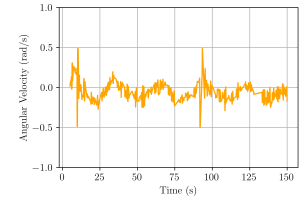


Fig. 16: Angular velocity - MPC

CONCLUSIONS

This work presents a low-cost, open-sourced SIL framework for Ackermann-steered autonomous vehicles by incorporating monocular vision, real-time telemetry, and flexible control experimentation. The platform allows for reliable testing of lane-tracking algorithms while maintaining low computational overhead.

Experiments with PID and MPC controllers show that the testbed successfully reflects the differences in control behavior: PID has a smaller tracking error, whereas MPC offers much smoother, constraint-aware control. The results presented herein validate this framework as a practical means of developing and comparing algorithms.

The overall system is set up to be easily extensible for future studies in multi-agent scenarios, learning perception, and onward development into Hardware-in-the-Loop tests.

REFERENCES

- [1] Monika Stoma, Agnieszka Dudziak, Jacek Caban, and Pawel Drożdźiel. The future of autonomous vehicles in the opinion of automotive market users. *Energies*, 14(16):4777, 2021.
- [2] Alireza Talebpour and Hani S Mahmassani. Influence of connected and autonomous vehicles on traffic flow stability and throughput. *Transportation research part C: emerging technologies*, 71:143–163, 2016.
- [3] José-Luis Blanco-Claraco, Borys Tymchenko, Francisco José Mañas-Alvarez, Fernando Cañadas-Aránega, Ángel López-Gázquez, and José Carlos Moreno. Multivehicle simulator (mvsim): Lightweight dynamics simulator for multiagents and mobile robotics research. *SoftwareX*, 23:101443, 2023.
- [4] Chaoyang Jiang, Hanqing Tian, Jibin Hu, Jiankun Zhai, Chao Wei, and Jun Ni. Learning based Predictive Error Estimation and Compensator Design for Autonomous Vehicle Path Tracking. In *2020 15th IEEE Conference on Industrial Electronics and Applications (ICIEA)*, pages 1496–1500, November 2020. ISSN: 2158-2297.
- [5] Rahul Kumar Bhadani, Jonathan Sprinkle, and Matthew Bunting. The CAT Vehicle Testbed: A Simulator with Hardware in the Loop for Autonomous Vehicle Applications, April 2018. arXiv:1804.04347 [cs].
- [6] Nikolaos Sarantinoudis, George Tsinarakis, Lefteris Doitsidis, Savvas Chatzichristofis, and George Arampatzis. A ROS-Based Autonomous Vehicle Testbed for the Internet of Vehicles. In *2023 19th International Conference on Distributed Computing in Smart Systems and the Internet of Things (DCOSS-IoT)*, pages 726–733, June 2023. ISSN: 2325-2944.
- [7] Ammar Elmoghazy, Khalid Elgazzar, and Sanaa Alwidian. A Real-World Testbed for V2X in Autonomous Vehicles: From Simulation to Actual Road Testing. In *2024 IEEE 8th International Conference on Fog and Edge Computing (ICFEC)*, pages 89–94, May 2024. ISSN: 2694-3255.
- [8] Naila Bouchemal and Sondes Kallel. Testbed of V2X infrastructure for autonomous vehicles. *Annals of Telecommunications*, 76(9):731–743, October 2021.
- [9] Liang Tang, Eric Hettler, Bin Zhang, and Jonathan DeCastro. A Testbed for Real-Time Autonomous Vehicle PHM and Contingency Management Applications. *Annual Conference of the PHM Society*, 3(1), September 2011.
- [10] Joaquin D. Labrado, Berat A. Erol, Jacqueline Ortiz, Patrick Benavidez, Mo Jamshidi, and Benjamin Champion. Proposed testbed for the modeling and control of a system of autonomous vehicles. In *2016 11th System of Systems Engineering Conference (SoSE)*, pages 1–6, June 2016.
- [11] Samy El-Tawab, Nathan Sprague, and Azeem Mufti. Autonomous Vehicles: Building a Test-bed Prototype at a Controlled Environment. In *2020 IEEE 6th World Forum on Internet of Things (WF-IoT)*, pages 1–6, June 2020.
- [12] Zheng Gong, Wuyang Xue, Ziang Liu, Yimo Zhao, Ruihang Miao, Rendong Ying, and Peilin Liu. Design of a Reconfigurable Multi-Sensor Testbed for Autonomous Vehicles and Ground Robots. In *2019 IEEE International Symposium on Circuits and Systems (ISCAS)*, pages 1–5, May 2019. ISSN: 2158-1525.
- [13] Jorge M. Vargas, Suleiman Alsweiss, Michael Jernigan, Abu Bony Amin, Marius Brinkmann, Joshua Santos, and Rahul Razdan. Development of Sensors Testbed for Autonomous Vehicles. In *2019 SoutheastCon*, pages 1–4, April 2019. ISSN: 1558-058X.
- [14] Armin Mokhtarian, Jianye Xu, Patrick Scheffe, Maximilian Kloock, Simon Schäfer, Heeseung Bang, Viet-Anh Le, Sangeet Ulhas, Johannes Betz, Sean Wilson, Spring Berman, Liam Paull, Amanda Prorok, and Bassam Alrifaae. A Survey on Small-Scale Testbeds for Connected and Automated Vehicles and Robot Swarms: A Guide for Creating a New Testbed [Survey]. *IEEE Robotics & Automation Magazine*, 32(3):146–163, September 2025.
- [15] Anil Gürses, Gautham Reddy, Saad Masrur, Özgür Özdemir, İsmail Güvenç, Mihail L. Sichitiu, Alphan Şahin, Ahmed Alkhateeb, Magreth Mushi, and Rudra Dutta. Digital Twins and Testbeds for Supporting AI Research with Autonomous Vehicle Networks. *IEEE Communications Magazine*, 63(4):56–62, April 2025.
- [16] Guizhen Yu, Zhangyu Wang, Xinkai Wu, Yalong Ma, and Yunpeng Wang. Efficient lane detection using deep lane feature extraction method. *SAE International Journal of Passenger Cars-Electronic and Electrical Systems*, 11(07-11-01-0006):57–66, 2017.
- [17] Yiqi Gao. *Model predictive control for autonomous and semiautonomous vehicles*. University of California, Berkeley, 2014.
- [18] Hengyang Wang, Biao Liu, Xianyao Ping, and Quan An. Path tracking control for autonomous vehicles based on an improved mpc. *IEEE access*, 7:161064–161073, 2019.
- [19] Shuo Cheng, Liang Li, Hong-Qiang Guo, Zhen-Guo Chen, and Peng Song. Longitudinal collision avoidance and lateral stability adaptive control system based on mpc of autonomous vehicles. *IEEE Transactions on Intelligent Transportation Systems*, 21(6):2376–2385, 2019.
- [20] Mohit Batra, John McPhee, and Nasser L Azad. Anti-jerk model predictive cruise control for connected electric vehicles with changing road conditions. In *2017 11th Asian Control Conference (ASCC)*, pages 49–54. IEEE, 2017.